Observation of Higher Order Parametric X-Ray Spectra in Mosaic Graphite and Single Silicon Crystals

R. B. Fiorito,[1,*] D. W. Rule,[1] X. K. Maruyama,[2] K. L. DiNova,[2] S. J. Evertson,[2] M. J. Osborne,[2] D. Snyder,[2] H. Rietdyk,[2] M. A. Piestrup,[3] and A. H. Ho[3]

[1]*Research and Technology Department, Naval Surface Warfare Center, Silver Spring, Maryland 20903*
[2]*Physics Department, Naval Postgraduate School, Monterey, California 93943*
[3]*Adelphi Technology Inc., Palo Alto, California 94301*

(Received 15 March 1993)

We have observed up to 8 orders (n) in the spectra of parametric x-radiation (PXR), in the range 5–40 keV, produced by the interaction of a 90 MeV electron beam with mosaic graphite and single silicon crystals. The measured yields and intensity ratios, $I(n \geq 2)/I(n=1)$, in graphite are not in agreement with the theory of PXR for mosaic crystals. In comparison, the ratios of intensities in silicon are close to the predictions of PXR theory for perfect crystals. The bandwidths of spectral lines measured in both silicon and graphite are in good agreement with theoretical predictions.

PACS numbers: 41.60.–m, 78.70.Ck

Parametric x-radiation (PXR) is produced when a charged particle interacts with a crystalline material. PXR can be interpreted as the coherent Bragg scattering of Weiszacker-Williams pseudophotons [1], associated with the Fourier components of the relativistic field of the particle, from the crystal planes. In this process, x rays are generated at twice the Bragg angle measured relative to the velocity vector of the particle.

Since first predicted in the early 1970's [1–3], a number of classical and quantum electrodynamical treatments of PXR have been developed, based on a kinematic point of view [4], and on the dynamical theory of x-ray diffraction [5–8]. PXR is highly directed, quasimonochromatic, tunable, polarized, and spectrally intense [6–10]. At small Bragg angles the PXR process is a particularly efficient bright source of hard x rays [8]. These properties make it potentially useful for a wide variety of applications such as materials analysis [11], microscopy, nanofabrication, and digital subtraction imaging [10]. Experimental studies of PXR from beams with energies from 25 to 900 MeV interacting with several types of *single* crystals have generally verified the predicted angular distribution, bandwidth, and polarization of PXR [12–18].

We report the first measurements of PXR spectra from a mosaic crystal [19], compression annealed pyrolytic graphite (CAPG), which has the highest measured x-ray reflectivity [20,21]. To our knowledge, this is also the first reported PXR measurement in a Bragg geometry. Caticha [8] has pointed out that in this case multiple scattering is reduced and therefore the PXR is produced by a higher quality beam than in a Laue geometry. We present a quantitative study of the yield of multiple order spectra in graphite, the ratio of intensities in silicon, and the bandwidths of PXR spectral lines, which show their dependence on the aperture of the detector.

The spectral-angular distribution [5,6] of PXR from a perfect crystal may be written as

$$\frac{\partial^3 N}{\partial\theta_x \partial\theta_y \partial\omega} = \frac{1}{\pi^2}\frac{e^2}{\hbar c}\frac{1}{\omega_B}|\chi_{10}|^2 e^{-2M}\frac{\theta_x^2\cos^2(2\theta_B)+\theta_y^2}{(\gamma^{-2}+\theta_x^2+\theta_y^2+|\chi_0|)^2}(1-e^{-L/L_a})\frac{1}{16\sin^4\theta_B(\theta_x/\tan\theta_B-\Delta\omega/\omega_B)^2+\rho_s^2}, \quad (1)$$

where θ_B is the Bragg angle, θ_x,θ_y are the angular displacements away from θ_B, in and out of the incidence plane, respectively, χ_0 is the mean dielectric susceptibility, χ_{10} is the structure factor, $\rho_s = \lambda/2\pi L_a(\omega)$, $L_a(\omega), L$ are the absorption and path lengths, respectively, and e^{-2M} is the squared Debye-Waller (DW) factor [21]. Equation (1) applies to each frequency $\omega_B(n)$ which satisfies the Bragg condition: $\omega_B(n) = n\pi c/d\sin\theta_B$, where d is the interplanar spacing of the set of crystal reflecting planes, and n is the spectral order.

To obtain the spectral distribution, we integrate Eq. (1) over the solid angle subtended by the detector, $d\Omega = \Delta\theta_x\Delta\theta_y$, where $\Delta\theta_x$ and $\Delta\theta_y$ are the angular fields of view in and out of the plane of observation, respectively. When $\Delta\theta_x \gg \rho_s$,

$$\frac{\partial N}{\partial\omega} = \frac{e^2}{\hbar c}\frac{|\chi_{10}|^2 e^{-2M}}{4\sin\theta_B\cos\theta_B}\frac{L_a(1-e^{-L/L_a})}{\pi c\theta_p}J_2(\alpha_y,u)S(\alpha_x-|u|), \quad (2)$$

where $J_2(\alpha_y,u)$ is obtained by straightforward integration of Eq. (1) over θ_y, and $u \equiv [(\omega-\omega_B)/\omega_B](\tan\theta_B)/\theta_p = \theta_x/\theta_p$. $S(\alpha_x-|u|)$ is the step function which is unity when its argument is positive and is zero otherwise. $\alpha_{x,y} = \Delta\theta_{x,y}/2\theta_p$, where $\theta_p = (\gamma^{-2}+|\chi_0|+\theta_s^2)^{1/2}$, and $\theta_s^2 = \theta_d^2+\theta_{\rm scat}^2+\theta_{\rm mos}^2$ approximates the effects of beam divergence, multiple scattering, and mosaicity [11]. In deriving Eq. (2), we have approximated the last factor in Eq. (1) by $(\pi/\rho_s)\delta[\theta_x-\tan\theta_B(\omega-\omega_B)/\omega_B]$, which correlates θ_x and $\omega-\omega_B$, and also connects the finite aperture of the detector

0031-9007/93/71(5)/704(4)$06.00

$\Delta\theta_x$ with the observed spectral bandwidth $\Delta\omega$. When $\Delta\theta_{x,y} \rightarrow \infty$, Eq. (2) reduces to Eq. (8) of Ref. [6].

Equations (1) and (2) are derived from a dynamical approach [5]; however, the last term in Eq. (1) and the use of the δ function are essentially kinematic approximations. Nitta [4] has shown that the kinematic formula is adequate for comparison with experiments when $\gamma^{-1} \gg |\chi_{10}|$, which is the case for our experiments. The role of the orientation of the crystal surface and the dispersion relationship for x rays has been clearly elucidated in a fully dynamical treatment by Caticha [7,8].

For most experimental situations, $\infty > \Delta\theta_x > \rho_s$. Then, if $\Delta\theta_x/\theta_p < \Gamma_2$, the FWHM of J_2, S limits the bandwidth in Eq. (2), i.e., $\Delta\omega \propto \Delta\theta_x$; otherwise, $\Delta\omega \propto \Gamma_2$. We shall refer to these situations as the *far case* and *near case,* respectively. Far case conditions apply to all the experiments previously reported.

We have observed the PXR spectra of a 90 MeV electron beam, produced by an S band rf linac producing 1 μs pulses at a rate of 60 pps, interacting with the $\langle 111 \rangle$ and $\langle 022 \rangle$ planes of silicon (Si) in a Laue geometry for the far case condition, and the $\langle 002 \rangle$ planes of mosaic graphite in a Bragg geometry for both far and near cases. Si crystals 20, 44, and 320 μm thick, and a 1.39 mm thick CAPG crystal (0.4° mosaic spread) manufactured by Union Carbide Inc. were used. In all the experiments reported here, $\theta_B = 22.5°$. PXR is observed at a fixed detector angle $2\theta_B = 45°$. The Si crystals are cut so that the $\langle 022 \rangle$ planes are oriented at 90° relative to the crystal face, whose normal is in the $\langle 200 \rangle$ direction. For the graphite, the $\langle 002 \rangle$ reflection planes are parallel to the face of the crystal.

The experimental arrangement is described in Ref. [17]. A 16 mm square, 5 mm thick Si(Li) detector enclosed by a 50 μm Be window is used to detect the x rays, and is located in air 1.0 m from the crystal for the far case, and 0.3 m away for the near case. A 0.001 in. thick Kapton window and a 1.4 cm air gap separated the vacuum from the detector window. A gated, multichannel analyzer is used to obtain the x-ray energy spectra. The calibration and resolution of the detector are determined by observing the x-ray fluorescence lines from a stack of titanium, yttrium, and tin foils placed in the beam path.

The absolute PXR yield (photons/electron), η, is obtained for graphite by integrating the number of photons in a given spectral peak and dividing by the number of electrons. X-ray fluorescence from a tin foil placed directly behind the crystal is detected along with the PXR spectra and used to calculate the beam current, which is kept at $\sim 4\times10^{-14}$ A to avoid double counting in the detector.

Figure 1 shows a plot of the raw PX spectrum from the $\langle 002 \rangle$ planes of graphite, for the far case. This spectrum exhibits a large number (8) of spectral orders observed and a very low background level. The presence of so many orders can be qualitatively explained by considering

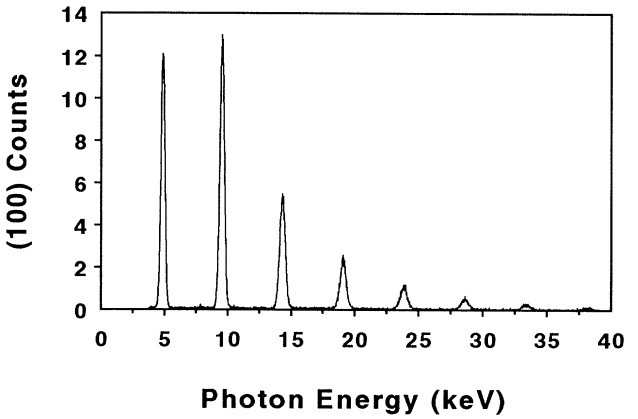

FIG. 1. Parametric x-ray spectrum from $\langle 002 \rangle$ planes of a mosaic graphite crystal at $\theta_B = 22.5°$.

the terms containing L_a and χ_{10} in Eq. (2). As the energy of the order increases, L_a increases so that for $n > 2$ the production becomes proportional to the path length L, since $L_a(\omega) > L$ for $E > 10$ keV. The term $|\chi_{10}|^2$ decreases with increasing energy, but not as fast as L_a increases.

The measured [22] and theoretical [23] yields ($\theta_s^2 \geq 0$) are given in Table I for a representative far case data set. The measured higher order ($n \geq 2$) yields are 2–200 times the calculated values for $\theta_s^2 > 0$, and 1.5–260 times the $\theta_s^2 = 0$ calculations for $n \geq 4$. Similar ratios are obtained for the near case. For the far case, $\eta_{\text{meas}}(1) < \eta_{\text{theo}}(1)$ when $\theta_s^2 > 0$, and $\eta_{\text{meas}} < \eta_{\text{theo}}$ for $n < 4$ when $\theta_s^2 = 0$. For the near case, $\eta_{\text{meas}}(1) = (2.6 \pm 1.3)\times10^{-5}$ photons per electron, which is larger than the far case value, as is expected. However, the theoretical first order values, 5.5×10^{-5} for $\theta_s^2 > 0$, and 8.0×10^{-5} for $\theta_s^2 = 0$ are again both larger than the measured values [24].

The values of θ_s^2 used in Eq. (2) to calculate the theoretical yields in Table I include $\theta_{\text{mos}}^2 = 5\times10^{-5}$, and θ_{scat}^2, which is obtained from the Bethe-Ashkin multiple scattering formula. To first order, $\theta_{\text{scat}}^2 \propto \langle x \rangle \equiv \int x e^{-x/L_a} dx / \int e^{-x/L_a} dx$, the effective crystal thickness,

TABLE I. Measured and theoretical PXR yields in graphite.

n	E (keV)	η_{meas} (N/elec) $\times10^{-6}$	$\eta_{\text{meas}}/\eta_{\text{theo}}$ $\theta_s^2 > 0$	$\eta_{\text{meas}}/\eta_{\text{theo}}$ $\theta_s^2 = 0$
1	4.88	1.67	0.3	0.13
2	9.53	1.72	2.1	0.36
3	14.29	0.85	5.6	0.79
4	19.08	0.42	11.7	1.54
5	23.88	0.23	23.4	3.04
6	28.68	0.13	48.8	6.18
7	33.56	0.07	97.8	12.3
8	38.44	0.03	204.6	260.0

which accounts for absorption in the crystal. In graphite, θ^2_{scat} varies from 8.4×10^{-6} at 5 keV to 8.8×10^{-5} at 40 keV, and exceeds 6.0×10^{-5} for energies ≥ 10 keV. The measured beam divergence at 90 MeV, $\theta_d^2=10^{-6} \ll \theta^2_{mos}, \theta^2_{scat}$ for all energies considered, and is negligible.

Figure 2 shows a comparison of the PXR spectra from the $\langle 111\rangle$ planes of single crystal Si for three different thicknesses. The 44 and 320 μm spectra show the $n=3$ and $n=4$ spectral lines but not the $n=2$ line. The selection rule for normal x-ray scattering for diamondlike, face centered cubic crystals such as silicon forbid the $n=2$ reflection. By analogy, the $n=2$ order should also be absent from PXR spectra, as our results indicate. Figure 2 also illustrates the effect of thickness on the intensity of higher order spectra. The appearance of the $\langle 333\rangle$ line at $\sim$15 keV, and the $\langle 444\rangle$ line at $\sim$21 keV, is due to the fact that $\eta \propto L$, since $L_a \gg L$ at these energies.

A comparison of measured and theoretical ratios of integrated intensities for each order is shown for Si in Table II. The measured ratios are much closer to the theoretical predictions than in mosaic graphite. For single crystal silicon, $\theta^2_{mos}=0$, and θ_s^2 contains only the θ^2_{scat} contribution. Table II shows that θ^2_{scat} has only a small effect on the calculated values in this case. In the calculation, allowance was made for the increased absorption for the $\langle 111\rangle$ asymmetric Laue reflections [8] (see Fig. 5 of Ref. [17]).

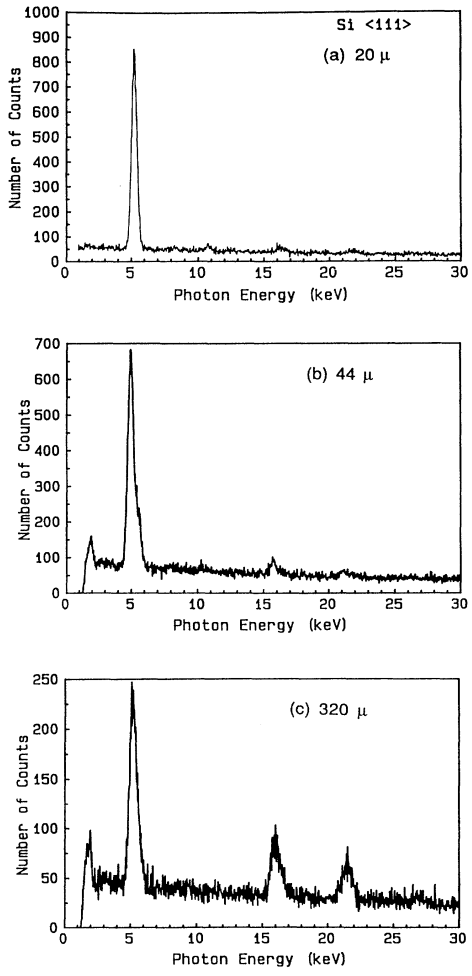

FIG. 2. Parametric x-ray spectra from $\langle 111\rangle$ planes of single Si crystals with thicknesses (a) 20 μm, (b) 44 μm, and (c) 320 μm.

We have not made a measurement of the yield for silicon. However, in Ref. [14], η has been measured at 900 MeV: $(1.55\pm0.3)\times10^{-6}$ photons/electron for the $\langle 111\rangle$ reflection at 12 keV ($\theta_B=9.5°$), and $(5.67\pm1.03)\times10^{-6}$ for the (220) reflection at 19 keV. Using Eq. (2) with $\theta_s^2=0$, we obtain 2.2×10^{-6} for the (111) reflection and 3.0×10^{-6} for the (220) reflection.

We have measured the percent bandwidths of all the spectral lines observed. Averaged over the energy range of observation, $\Delta\omega/\omega_B=(3.2\pm1.5)\%$ (graphite) and $(4\pm1.8)\%$ (Si) for the far case, and $(6.1\pm3.2)\%$ (graphite) for the near case. These values are in excellent agreement with the predictions of Eq. (2): 3.8% and 7% for the far and near cases, respectively.

In view of the much higher values of the measured yields in comparison to the predicted values in mosaic graphite, we have focused on the theoretical treatment of mosaicity as a possible source of discrepancy between PXR theory and experiment. Reference [5] presents the only theory of PXR production in mosaic crystals, and predicts essentially the same result as the perfect crystal expressions used in the present analysis.

In order to find possible approaches to improve the theory for mosaic crystals, we have examined primary (PE) and secondary extinction (SE) effects, which have been shown to affect the x-ray reflectivity of CAPG [21]. The SE correction factors (C_{SE}) for the $n=1$–6 orders in CAPG range from 0.61 to 0.98. A C_{SE} improves the comparison with experiment for $n=1$, but the higher order data cannot be brought into agreement with theory by applying a C_{SE} alone. We have also calculated the PE

TABLE II. Ratios of integrated spectral intensities in silicon.

t (μm)	Plane	E (keV)	$I(n)/I(1)$ (meas)	$I(n)/I(1)$ (theo) $\theta_s^2=0$	$I(n)/I(1)$ (theo) $\theta_s^2>0$
44	(022)	8.18	1.000		
	(044)	16.97	0.084	0.074	0.074
320	(022)	8.21	1.000		
	(044)	17.16	0.162	0.20	0.12
44	(111)	4.56	1.000		
	(333)	15.30	0.033	0.069	0.069
	(444)	20.80	0.021	0.016	0.016
320	(111)	4.72	1.00		
	(333)	15.62	0.25	0.30	0.35
	(444)	21.15	0.20	0.093	0.11

corrections, and found that they cannot explain the discrepancy between the theoretical and measured yields when reasonable values for the microcrystallite thickness were assumed [20,21].

In view of these results, it is clear that the present understanding of PXR production in mosaic crystals is incomplete and insufficient to explain the measured intensities in mosaic graphite. We are currently pursuing other approaches to improve the theory of PXR in mosaic structures. Experiments with crystals with larger mosaic spreads are currently in progress.

This work was partially supported by a DOE SBIR Contract (No. DE-FG03-91ER81099), DNA, and the Naval Postgraduate School.

*Electronic address: rfiorit@nswc-wo.navy.mil

[1] M. L. Ter-Mikaelian, *High Energy Electromagnetic Processes in Condensed Media* (Wiley-Interscience, New York, 1972), pp. 332-335.

[2] V. G. Baryshevsky and I. D. Feranchuk, Zh. Eksp. Teor. Fiz. **61**, 944 (1971); **64**, 1190 (1973) [Sov. Phys. JETP **34**, 502-504 (1972); **37**, 605 (1973)].

[3] G. M. Garibyan and C. Yang, Zh. Eksp. Teor. Fiz. **61**, 930-943 (1971) [Sov. Phys. JETP **34**, 495 (1972)].

[4] H. Nitta, Phys. Lett. A **158**, 270 (1991); Phys. Rev B **45**, 7621-7626 (1992).

[5] A. M. Afana'sev and M. A. Aginyan, Zh. Eksp. Teor. Fiz. **74**, 570-579 (1978) [Sov. Phys. JETP **47**, 300-305 (1978)].

[6] I. D. Feranchuk and A. V. Ivanshin, J. Phys. (Paris) **46**, 1981-1986 (1985).

[7] A. Caticha, Phys. Rev. A **40**, 4322-4329 (1989).

[8] A. Caticha, Phys. Rev. B **45**, 9541-9550 (1992).

[9] V. G. Baryshevsky and I. D. Feranchuk, Nucl. Instrum. Methods Phys. Res., Sect. A **228**, 490-495 (1985).

[10] R. B. Fiorito, D. W. Rule, M. A. Piestrup, Q. Li, A. H. Ho, and X. K. Maruyama, Nucl. Instrum. Methods Phys. Res., Sect. B **79**, 758-761 (1993).

[11] A. V. Ivaskin and I. D. Feranchuk, Kristallografiya **34**, 39-46 (1989) [Sov. Phys. Crystallogr. **34**, 21-24 (1989)].

[12] S. A. Vorob'ev *et al.*, Pis'ma Zh. Eksp. Teor. Fiz. **41**, 3-6 (1985) [JETP Lett. **41**, 1-4 (1985)].

[13] V. G. Baryshevsky *et al.*, J. Phys. D **19**, 171-176 (1986).

[14] Yu. N. Adishchev *et al.*, Nucl. Instrum. Methods Phys. Res., Sect. B **21**, 49-55 (1987).

[15] Yu. N. Adishchev *et al.*, Zh. Eksp. Teor. Fiz. **93**, 1943 (1987) [Sov. Phys. JETP **66**, 1107-1111 (1987)].

[16] A. V. Shchagin *et al.*, Phys. Lett. A **148**, 485-488 (1990).

[17] D. W. Rule, R. B. Fiorito, M. A. Piestrup, C. K. Gary, and X. K. Maruyama, Proc. SPIE Int. Soc. Opt. Eng. **1552**, 240 (1991).

[18] Yu. N. Adishchev *et al.*, Nucl. Instrum. Methods Phys. Res., Sect. B **44**, 130-136 (1989).

[19] An earlier unsuccessful attempt to observe PXR in LiF and NaI mosaic crystals was made by Luke C. Yuan *et al.*, Nucl. Instrum. Methods Phys. Res., Sect. A **234**, 426 (1985).

[20] A. W. Moore, in *Chemistry and Physics of Carbon*, edited by P. L. Walker and P. A. Thrower (Marcel Dekker, New York, 1981), Vol. 17, pp. 233-286.

[21] M. Chabot, P. Nicholai, K. Wohrer, J. Rozet, A. Chetioui, D. Vernhet, and M. Politis, Nucl. Instrum. Methods Phys. Res., Sect. B **61**, 377-384 (1991).

[22] The estimated error in the far case measured yields is $\pm 35\%$.

[23] During a typical run (~ 2 h), the temperature rise of the crystal above room temperature is less than 0.01 K and is negligible. The DW factors used in Eq. (2) are computed at 293 K using the data of Ref. [21].

[24] The experimental yields presented above are obtained by integrating the number of counts over the bandwidth of each line and correcting this value for the absorption of the Kapton window, the air gap, the Be window, and the efficiency of the Si(Li) detector. The correction factors are calculated at the central energy of each line.